Advanced Mathematical Models & Applications
Vol.10, No.2, 2025, pp.347-362
https://doi.org/10.62476/amma.102347

DYNAMIC OPTIMIZATION OF A CRANK-CONNECTING ROD SYSTEM USING A FLYWHEEL: A MATHEMATICAL APPROACH

Samuel Fernando Enríquez Guzmán*

Electronic Engineer and Mathematics Professor, Arequipa, Peru

Abstract. Rotational systems exhibit fluctuations, which do not permit the correct operation in the presence of underused power. The system is being modelled with flywheel that permit analysing its dynamic behaviour and evaluating how flywheel improves stability and efficiency. The mathematical model studies the moment of inertia, the resulting torque acting during motion, the flywheel's impact on reducing angular velocity and torque's fluctuations, optimizing energy use, the dynamic behaviour by solving nonlinear differential equations that describe angular acceleration. The objective is to understand how the inclusion of a flywheel helps smooth out torque oscillations and improves the system's energy efficiency. An inverse dynamic analysis of the system is performed, solving differential equations of motion. Principles of energy conservation, kinematics, and rigid-body dynamics are used to model. Simulations are presented to evaluate the variation in angular velocity and the effect of the flywheel on system stability. The system without a flywheel exhibits fluctuations in angular velocity and input torque; so, with the flywheel, the angular velocity is more stable and the torque is reduced. Finally, the relationship between the system's moment of inertia and the flywheel allows for the design of a more efficient system, improving the system's energy efficiency.

Keywords: nonlinear differential equations, inverse dynamic analysis, inertia, torque, angular acceleration.
AMS Subject Classification: 34-02.
Corresponding author: Samuel Enríquez, Electronic Engineer and Mathematics Professor, Ca. Miguel Forga N246. Z.I. Senati Industrial Park, Arequipa, Peru, Tel.: +51 935390928, e-mail: *senriquezg@unsa.edu.pe*
Received: 31 December 2024; Revised: 15 March 2025; Accepted: 10 April 2025; Published: 4 August 2025.

1 Introduction

Fluctuations were observed along the rotational axis. Yes, fluctuations are present on the rotational axis. The significance of this phenomenon is that spurious oscillations will generate very large amounts of power that would be inefficient because, most of the time, it would be underutilized. Increasing the inertia of the flywheel can mitigate fluctuations in the external torque (Lindner & Strauch, 2018). Flywheel devices are mechanical elements that store the rotational kinetic energy accumulated during acceleration, and are released when a given load is applied. To do this, it is necessary to analyze the torque experienced by the shaft or crankshaft T_L so that it is as similar as possible to the constant torque delivered by the engine T_M, then you must remember and apply the law of conservation of matter of Mikhail Vasilievich Lomonosov and Antoine Laurent Lavoisier (Zhang et al., 2025) and the law of conservation of energy of Rudolf Clausius and William Thomson also known as Lord Kelvin (Lindner & Strauch, 2018) according to which it is established that: energy is neither created nor destroyed, it only transforms. Similarly, Sir Isaac Newton's second law must be used (Coelho, 2018) which establishes that a body subjected to a force other than zero has acceleration in the same direction as the force, and its module is acceleration = force/mass, performing an analysis in its rotational form for the moment of inertia of the mechanism. In the crank-connecting rod system, a certain shape was taken on by the torque during force analysis (Khudhair et al., 2024). The torque exhibited a significant oscillation. Although there was an average torque value, the maximum torque was higher than the average. A very large amount of inefficient power is mostly underutilized as a consequence of the motor sizing for the maximum torque because the power is equal to the torque multiplied by the angular velocity. The accumulation of kinetic energy and delivery of kinetic energy when required are carried out through a mechanical device, which is a flywheel that allows the motor to be sized for an average torque rather than a maximum torque.

Mathematical modeling does not consider the structure with translational movement (Zhao et al., 2022), nor the mass reduction method (Reyes et al., 2017), almost with a simulation approximation (Beckers et al., 2021), nor is the analysis in complex numbers reviewed (Drápal & Novotný, 2017), nor only the horizontal displacement or the angular velocity in a vectorial way (Lu et al., 2025), establishing a single axis for the system (Chmielowiec et al., 2025; Urbaś & Stadnicki, 2025) considering that what is sought is an analysis model of forces and moments of inertia that act through the center of gravity of the moving elements.

In addition, a topological optimization of an internal combustion engine connecting rod has been carried out with the aim of reducing its component material while maintaining its mechanical properties (Carrillo, 2022), who reported a 26.72% decrease in mass of a connecting rod using the finite element method, with an improvement in the strength-weight ratio without altering the fundamental dimensions of the component; as well as another multiphase optimization on generative design of an Internal Combustion engine connecting rod through Inventor Software (Beltrán, 2022), whose implementation was given to redesign a Mazda BT-50 Diesel engine connecting rod, which made it possible to reduce the weight of the connecting rod while maintaining its mechanical properties. In addition, the application of composite materials in the composition of flywheels is established to increase the energy storage capacity without significantly increasing its weight (Premkumar et al., 2021). On the other hand, Equimake has developed electric motors based on flywheel technology used in Formula 1, with high power density and efficiency (Bayram & Samuel, 2025). Additionally, advanced flywheel systems have been developed with low friction losses, employing magnetic or air bearings to reduce friction and improve efficiency (Rasha & Machicao, 2023).

1.1 Description of the Mathematical Model

The mathematical model considers the moment of inertia of the mechanism, the equations of motion of the connecting rod and crank, and the flywheel equation. Second-order nonlinear differential equations are included that describe the angular acceleration of the system. The model is compared with results obtained without a flywheel, showing that the flywheel reduces torque fluctuations.

2 Method

An inverse dynamic analysis of the system is performed, solving differential equations of motion. Principles of energy conservation, kinematics, and rigid-body dynamics are used to model the system. Simulations are also presented to evaluate the variation in angular velocity and the effect of the steering wheel on system stability.

2.1 Inertia's moment of crank-connecting rod mechanism

From Fig. 1 and 2 $\sum M_{mass} = \sum M_{inertial}$, considering (+) clockwise:

$$B_x.\tfrac{a}{2}.\sin\alpha + B_y.\tfrac{a}{2}.\cos\alpha \text{ - } A_y.\tfrac{a}{2}.\cos\alpha \text{ - } A_x.\tfrac{a}{2}.\sin\alpha + T = \bar{I}_1\ddot{\alpha}.$$

Additionally, there is $\sum Fv_{mass} = \sum Fv_{inertial}$. Considering (+) upward forces.

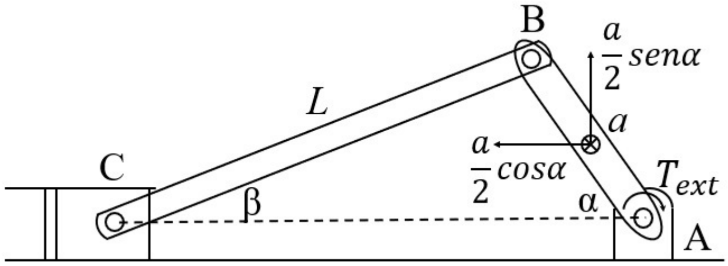

Figure 1: Position vector components in the basic crank diagram

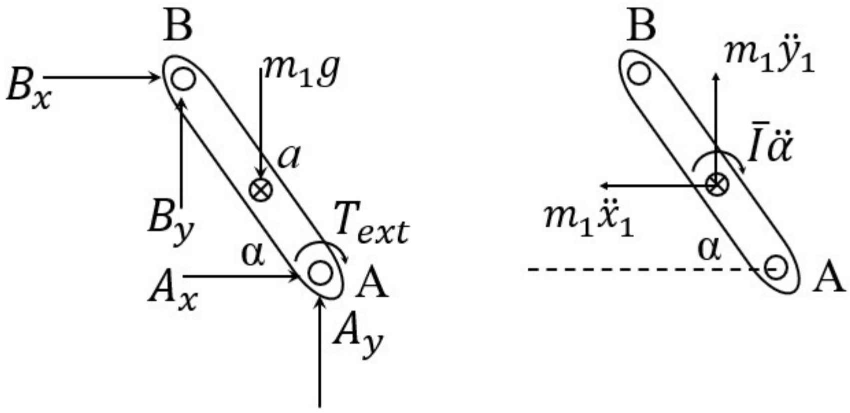

(a) External forces (b) Inertial forces, $T_{Inertial} = \bar{I}_1.\ddot{\alpha}$

Figure 2: Free body diagram of crank a

$\sum F_y = m_1.\ddot{y}$:

$$B_y + A_y - m_1.g = m_1.\ddot{y}.$$

In addition, there is $\sum Fh_{mass} = \sum Fh_{inertial}$. Considering positive (+) left forces.

$\sum F_x = m_1.\ddot{x}$:

$$-B_x - A_x = m_1.\ddot{x}.$$

Building equations of motion:

$\sum M_{CM} = \bar{I}\ddot{\alpha}$:

$$B_x.\tfrac{a}{2}.\sin\alpha + B_y.\tfrac{a}{2}.\cos\alpha \text{ - } A_y.\tfrac{a}{2}.\cos\alpha \text{ - } A_x.\tfrac{a}{2}.\sin\alpha + T = \bar{I}_1\ddot{\alpha}.$$

$\sum F_y = m_1.\ddot{y}$:

$$B_y + A_y - m_1.g = m_1.\ddot{y}.$$

$\sum F_x = m_1.\ddot{x}$:

$$-B_x - A_x = m_1.\ddot{x}.$$

According to Fig. 1 and 3, the damping forces always oppose motion.
B_x and B_y are external forces on AB, but in the opposite direction.
Displacement of the plunger from point C to point A: $x_c = a\cos\alpha + L\cos\beta$.
Velocity generated from point C to point A: $\frac{dx_c}{dt} = \dot{x} =$ - $a\dot{\alpha}\sin\alpha - L\dot{\beta}\sin\beta$.
In this instance, Block C's leftward-pointing velocity was assumed to be positive.

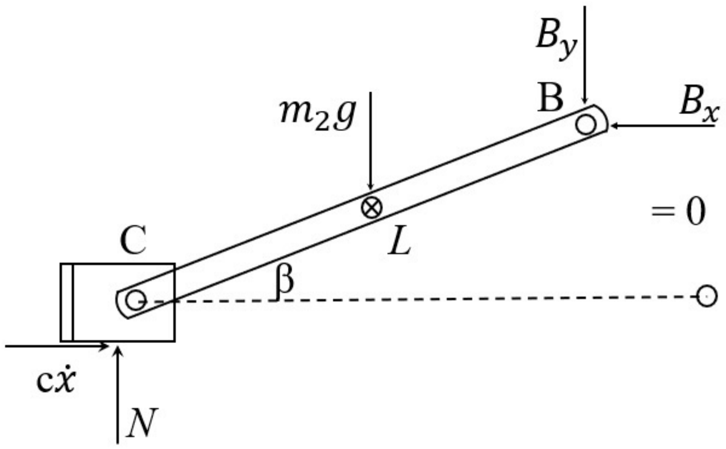

Figure 3: Free body diagram of bar BC or connecting rod L

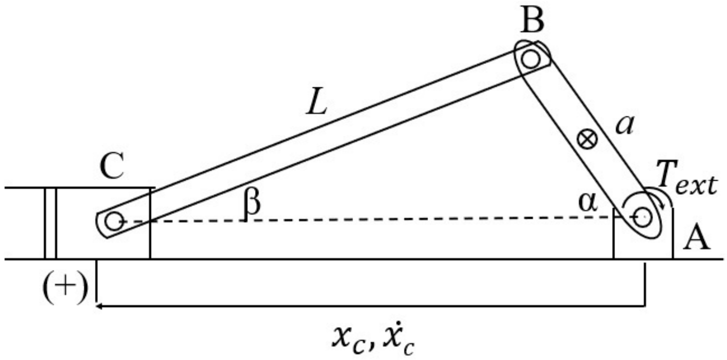

Figure 4: Positive direction of velocity $\dot{x}_c$ of the plunger C (piston or cylinder) to the left

As shown in Fig. 4, the friction force F_F (Liang et al., 2021) moves in the opposite direction. If the damping type is assumed to be viscous, then it is proportional to the velocity $\dot{x}_c$ of the plunger at point C according to $F_F = c.\dot{x}_c$; where c is the coefficient of friction or proportion constant.

Then, equations of motion for the system are expressed by:

$\sum M_{CM} = 0$:

$$B_x.\tfrac{L}{2}.\sin\beta \text{ - } B_y.\tfrac{L}{2}.\cos\beta \text{ - } N.\tfrac{L}{2}.\cos\beta + F_F.\tfrac{L}{2}.\sin\beta = 0.$$

$\sum Fx = 0$:

$$B_x \text{ - } F_F = 0.$$

$\sum F_y = 0$:

$$N - m_2.g \text{ - } B_y = 0.$$

The equations following the laws of motion for each rigid body are expressed by:

$$B_x.\frac{a}{2}.\sin\alpha + B_y.\frac{a}{2}.\cos\alpha - A_y.\frac{a}{2}.\cos\alpha - A_x.\frac{a}{2}.\sin\alpha + T - \bar{I}_1.\ddot{\alpha} = 0. \tag{1}$$

$$B_y - m_1g + A_y - m_1.(-\frac{a}{2}.\dot{\alpha}^2.sin\alpha + \frac{a}{2}.\ddot{\alpha}.\cos\alpha) = 0. \tag{2}$$

$$-B_x - A_x - m_1(-\frac{a}{2}.\dot{\alpha}^2.\cos\alpha - \frac{a}{2}.\ddot{\alpha}.\sin\alpha) = 0. \tag{3}$$

$$\frac{L}{2}.B_x.\sin\beta - \frac{L}{2}.B_y.\cos\beta - N.\frac{L}{2}.cos\beta + F_F.\frac{L}{2}.\sin\beta = 0. \tag{4}$$

$$B_x - F_F = 0. \tag{5}$$

$$N - m_2.g - B_y = 0. \tag{6}$$

Being the unknowns A_x, A_y, B_x, B_y, N, $\ddot{\alpha}$

From (3):

$$A_x = -m_1(-\frac{a}{2}.\dot{\alpha}^2.cos\alpha - \frac{a}{2}.\ddot{\alpha}.\sin\alpha) - B_x. \tag{7}$$

From (2):

$$A_y = m_1(-\frac{a}{2}.\dot{\alpha}^2.sin\alpha + \frac{a}{2}.\ddot{\alpha}.\cos\alpha) + m_1.g - B_y. \tag{8}$$

From (4): $B_x = 0$:

$$B_y = \frac{B_x.\sin\beta - N.\cos\beta + F_F.sin\beta}{\cos\beta}. \tag{9}$$

From (4): $F_F = 0$:

$$B_x = \frac{B_y.\cos\beta + N.\cos\beta}{\sin\beta}. \tag{10}$$

(7), (8), (9), (10) in (1):

$$\ddot{\alpha} = \frac{2(2T + 2F_F.a(\cos\alpha.\tan\beta + \sin\alpha) - m_1.g.a.\cos\alpha)}{(4I_1 + m_1.a^2)}. \tag{11}$$

This becomes a highly nonlinear second-order differential equation for the angular acceleration provided by a crank-connecting rod system. From (3) obtaining A_x and replacing (5):

$$A_x = m_1.\frac{a}{2}.(\dot{\alpha}^2.\cos\alpha - \ddot{\alpha}.\ sin\alpha) - F_F. \tag{12}$$

From (2):

$$A_y = -m_1.\frac{a}{2}.(\dot{\alpha}^2.\sin\alpha - \ddot{\alpha}.\cos\alpha) + m_1.g - B_y. \tag{13}$$

If:

$$\tan\beta = \frac{N}{F_F}. \tag{14}$$

Clearing N:

$$N = F_F.\tan\beta. \tag{15}$$

From (6):

$$B_y = N - m_2.g. \tag{16}$$

(15), (16) in (13):

$$A_y = -m_1.\frac{a}{2}.(\dot{\alpha}^2.sin\alpha - \ddot{\alpha}.cos\alpha) + (m_1 + m_2).g - F_F.\tan\beta. \tag{17}$$

By law of sines:

$$\frac{L}{\sin\alpha} = \frac{a}{\sin\beta} \tag{18}$$

Showing β:

$$\beta = arcsen(\tfrac{a}{L}.\sin\alpha).$$

Deriving (18) in linear form with respect to time:

$$\tfrac{d(L.\sin\beta)}{dt} = \tfrac{d(a.\sin\alpha)}{L}.$$

From it is obtained:

$$L.\dot{\beta}.\cos\beta = a.\dot{\alpha}.\cos\alpha.$$

Clearing $\dot{\beta}$:

$$\dot{\beta} = \frac{a.\dot{\alpha}.\cos\alpha}{L.\cos\beta}. \tag{19}$$

Being:
α: Angular displacement of crank a in rad.
$\dot{\alpha}$: Angular velocity of crank a in rad/s.
$\ddot{\alpha}$: Angular acceleration of crank a in rad/s^2.
β: Angular displacement of connecting rod L in rad.
$\dot{\beta}$: Angular velocity of connecting rod L in rad/s.
$\ddot{\beta}$: Angular acceleration of connecting rod L in rad/s^2.
$\dot{x}_c$: displacement of plunger from point C to point A.
$\dot{x} = \frac{dx}{dt}$ = - $\frac{a}{2}.\dot{\alpha}.\sin\alpha$: speed of the plunger from point C to point A.
$\ddot{x} = \frac{d\dot{x}}{dt}$ = - $\frac{a}{2}.\dot{\alpha}^2.\cos\alpha$ - $\frac{a}{2}.\ddot{\alpha}.\sin\alpha$: acceleration of the plunger from point C to point A.
y = $\frac{a}{2}.\sin\alpha$: displacement of mass center of crank a of mass m_1.
$\dot{y} = \frac{dy}{dt}$ = + $\frac{a}{2}.\dot{\alpha}.\cos\alpha$: velocity of mass center of crank a of mass m_1.
$\ddot{y} = \frac{d\dot{y}}{dt}$ = - $\frac{a}{2}.\dot{\alpha}^2.\sin\alpha$ + $\frac{a}{2}.\ddot{\alpha}.\cos\alpha$: acceleration of mass center of crank a of mass m_1.

Author contribution: Using the kinematic conditions corresponding to $\ddot{\alpha} = 0$ implies that if

In (1):

$$\bar{I}_1.\ddot{\alpha} = 0. \tag{20}$$

In (2):

$$+\frac{a}{2}.\ddot{\alpha}.\cos\alpha = 0. \tag{21}$$

In (3):

$$-\frac{a}{2}.\ddot{\alpha}.\sin\alpha = 0. \tag{22}$$

In (6):

$$m_2.g = 0. \tag{23}$$

Subsequent to inverse dynamic analysis, it was determined that $\dot{\alpha}$ remained constant, indicating that $\ddot{\alpha} = 0$. From the two-dimensional dynamic analysis, the system of equations (1),(2),(3),(4),(5), and (6) results in

$$B_x.\frac{a}{2}.\sin\alpha + B_y.\frac{a}{2}.\cos\alpha - A_y.\frac{a}{2}.\cos\alpha - A_x.\frac{a}{2}.\sin\alpha + T = 0. \tag{24}$$

$$B_y - m_1.g + A_y - m_1(-\frac{a}{2}.\dot{\alpha}^2.\sin\alpha) = 0. \tag{25}$$

$$-B_x - A_x - m_1(-\frac{a}{2}.\dot{\alpha}^2.\cos\alpha) = 0. \tag{26}$$

$$\frac{L}{2}.B_x.\sin\beta - \frac{L}{2}.B_y.\cos\beta – N.\frac{L}{2}.\cos\beta + F_F.\frac{L}{2}.\sin\beta = 0. \tag{27}$$

$$B_x - F_F = 0. \tag{28}$$

$$N - B_y = 0. \tag{29}$$

To satisfy the condition $\dot{\alpha}$ as constant, the magnitude of the external load is sought to satisfy the condition α as a constant. In this case, the input torque is shown as a crank angle function, that is, as a function of the angular displacement α of the crank.

From (25), we obtain A_y, from (26), clearing A_x, both of which are replaced by in (24).

$$T = -\frac{a[2.F_F.\sin(\alpha+\beta) - m_1.g.\cos\alpha.cos\beta]}{2.\cos\beta}. \tag{30}$$

2.2 Building a flywheel

The flywheel has different shapes depending on its geometry, which corresponds to its size, to satisfy design requirements (Nkomo & Alugongo, 2024; Hu et al., 2021). These four models corresponded to the geometry of the flywheel for small discs. A constant-stress disk flywheel corresponds to a model with internal mass, where the thickness varies as the radius increases. The second model corresponds to a disk with an internal mass in the form of a variable-thickness disk with a constant effort. The third cross-sectional model of the flywheel had an internal mass, in which the thickness changed in a conical form. The fourth model is a section of the flywheel that corresponds to a flywheel with an internal mass in the form of a disk with a previously calculated radius and a constant thickness. The other four models have geometries with a large amount of inertia. First, the structure of the flywheel corresponds to that of a flywheel without an internal mass close to the axis of rotation, in the shape of a ring, where the thickness is constant. The second is structured by a flywheel section, which corresponds to a model without an internal mass in the form of a disc of variable thickness. The third section corresponds to a model without an internal mass, where the thickness varies in the middle section and maintains the greatest mass in the section closest to and furthest from the axis of rotation in the shape of the wheel. The fourth model of this second classification is structured as a section of a flywheel, which corresponds to a massless structure in the form of a disk with a previously calculated radius of constant thickness without mass in a section very close to the axis of rotation.

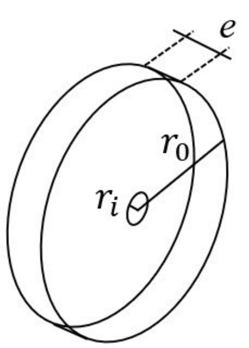

Figure 5: Flywheel with internal mass and constant thickness

Although there are many three-dimensional geometric shapes of flywheels, a dimensioning flywheel with a constant thickness was considered, as shown in Fig. 5.

Where:
r_i = internal radius of flywheel through which shaft passes.
r_0 = external radius of the flywheel covering the entire mass.
e = thickness of the flywheel with internal mass, which is constant.

Parameters e and r_0 are typically employed because r_i is typically recognized. It is necessary to analyze how e and r_0 vary to satisfy the amount of inertia that must be assigned to the mechanical system, while keeping the cost as low as possible. Because they are manufactured with bars, the larger the diameter of the bar, the higher is the cost. Normally, cost is always associated with mass as a measure. In general, the value is affected by the type of material, availability, weight, and ease of manufacturing. However, mass significantly influences the costs. The aim was to make the mass as small as possible and to satisfy the design requirements. When designing a flywheel, it is important to consider whether the moment of inertia is appropriate, and whether the mass is as small as possible. The final shape of the flywheel depends on aspects such as material availability and manufacturing cost. In general, the goal is to satisfy all the engineering requirements and achieve the lowest possible cost.

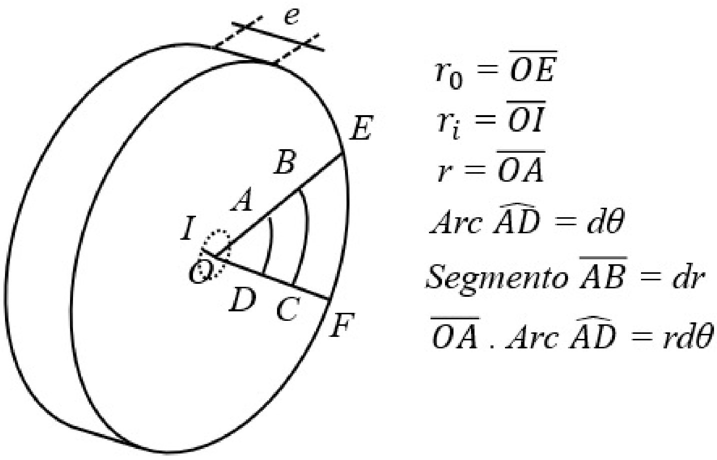

Figure 6: Differential elements in a flywheel of mass m

According to Fig. 6, in this case the moment of inertia is:

$$I = \int r^2.dm. \tag{31}$$

In mass segment ABCD, the area differential is:

$$dA = r.d\theta.dr. \tag{32}$$

The volume differential is:

$$dV = e.dA = e.r.d\theta.dr. \tag{33}$$

The mass differential is:

$$dm = \rho.dV = \rho.e.r.d\theta.dr. \tag{34}$$

(34) in (31):

$$I = \int_0^{2\pi} \int_{r_i}^{r_0} r^2.\rho.e.r.d\theta.dr.$$

Performing the angular integral:

$$I = 2\pi.\rho.e \int_{r_i}^{r_0} .r^3 dr.$$

Performing the linear integral:

$$I = \frac{1}{2}.\pi.\rho.e.(r_0^4 - r_i^4). \tag{35}$$

From (34):

$$m = \int_0^{2\pi} \int_{r_i}^{r_0} \rho.e.r.d\theta.dr.$$

Performing the angular integral:

$$m = 2.\pi.\rho.e \int_{r_i}^{r_0} r.dr.$$

Performing the linear integral:

$$m = \pi.\rho.e(r_0^2 - r_i^2). \tag{36}$$

The mass of the flywheel, which depends on ρ, e, r_o and, cannot be considered.
From (35):

$$r_0 = \sqrt[4]{\frac{2I}{\pi.\rho.e} + r_i^4}. \tag{37}$$

2.3 Finding kinetic energy

To determine the kinetic energy, the area under the curved line of the graph corresponding to the input torque of the system with and without the flywheel must be considered by using the following relationship (Akan & Chaparro, 2024):

$$E = Asin(\alpha), lowerlimit, upperlimit. \tag{38}$$

Where:
A: Amplitude of the curved line.
α: crank angle at which angular velocity occurs.
lower limit: Initial point for area analysis.
upper limit: Final point for area analysis.

Next, the variation in kinetic energy is:

$$\triangle E_C = E_{\dot{\alpha}} max - E_{\dot{\alpha}} min. \tag{39}$$

2.4 Finding the coefficient of fluctuation of the angular velocity

Consider the coefficient of fluctuation of the angular velocity with respect to the average value, calculated by

$$k = \frac{\dot{\alpha}_{max} - \dot{\alpha}_{min}}{\dot{\alpha}_{prom}}. \tag{40}$$

2.5 Finding the inertial components

The inertia of the system is:

$$I_{system} = \frac{|\triangle E_c|}{k.\dot{\alpha}^2_{prom}}. \tag{41}$$

The inertia of the crank is determined by:

$$I_{crank} = \frac{1}{3}.m_1.a^2. \tag{42}$$

Then the inertia of the flywheel becomes:

$$I_{flywheel} = I_{system} - I_{crank}. \tag{43}$$

(43) is considered for calculating the relationship between the moment of inertia of the system and the moment of inertia of the crank expressed in $kg.m^2$.
The inertia of the flywheel is the actual inertia to be considered in which the participation of the inertia of the system acts as a minuend and that of the crank acts as a subtrahend. This allows the inertia distribution to be determined, such that the movement is smoothed. The analysis of the crank-connecting rod system to be performed will be using a crank of length 0.2 $meters$ and mass $m_1 = 1.6$ kg, a connecting rod L of length 0.6 $meters$, considering a viscous friction constant c = 0.00001, acceleration of gravity $g = 9.81$ m/s^2, a material density of mass m plain carbon steel $\rho = 7850$ kg/m^3 (Steau et al., 2020), an internal radius r_o of the flywheel = 0.01 $meters$.

3 Results

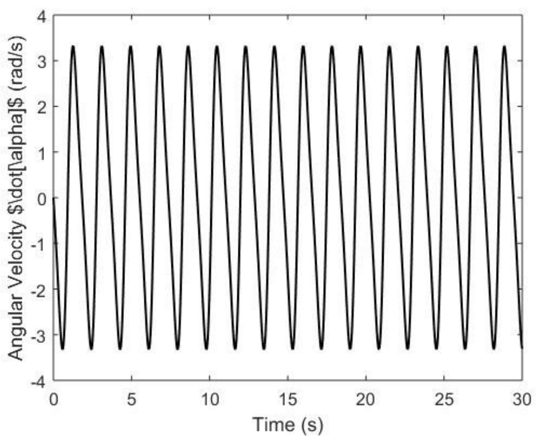

Figure 7: $\dot{\alpha}$ Angular velocity of crank a in rad/s

According to Fig. 7, for the crank a of mass $m_1 = 1.6$ Kg, of length 0.2 $meters$, working with a connecting rod L of length 0.6 $meters$, considering the friction coefficient $c = 0.00001$ and an acceleration of gravity $g = 9.81 m/s^2$, we have $\dot{\alpha} \neq 0$, with which the system moves steadily and does not stop, preventing under-damped motion (Kaveh & Ghazaan, 2017; Campanelli et al., 2020) which implies that the torque $T = 1.20$ $Newton.meter$ does have enough force to move the system in a permanent regime (Zhang et al., 2024) as an accumulation of self-sustained oscillations.

According to Fig. 8, for the crank working with a connecting rod L, under the same conditions, we have $\ddot{\alpha} \neq 0$, stable motion is obtained so the torque $T = 1.20$ $Newton.meter$ does have enough force to move the system in a permanent regime (Zhang et al., 2024) as an accumulation

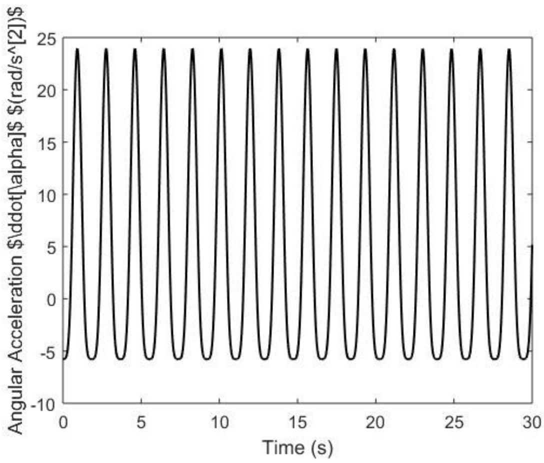

Figure 8: $\ddot{\alpha}$ Angular acceleration of the crank a in rad/s^2

of self-sustained oscillations. Note that the behavior of the angular acceleration $\ddot{\alpha}$ corresponding to the angular displacement carried out on the crank is opposite to the behavior of the angular velocity of the moving piece; that is, as the angular velocity increases, the angular acceleration decreases, and vice versa.

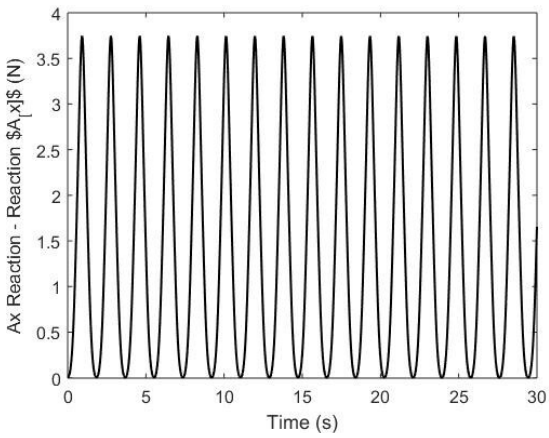

Figure 9: Resulting reaction on the x axis on the system

According to Fig. 9, for crank a with the same characteristics described and under the same conditions, a resulting reaction on the x axis different from zero is obtained, denoted by $R_x \neq 0$, with a maximum value of 3.8 $Newtons$ and a minimum value $R_x$min of $zero$, the behavior it presents is similar to that of the angular acceleration $\ddot{\alpha}$ corresponding to crank a, which leads to a moving system that does not stop, so the torque $T = 1.20$ $Newton.meter$ does have enough force to move the system in permanent regime.

According to Fig. 10, for crank a with the same characteristics described and under the same conditions, a resulting reaction on the y axis different from zero is obtained, denoted by $R_y \neq 0$, with a maximum value $R_y$max of 17.8 $Newtons$ and a minimum value $R_y$min of 14.8 $Newtons$, the behavior is similar to that of the angular acceleration $\ddot{\alpha}$ corresponding to crank a with the difference of double cycle with respect the resultant component R_x; this is because the route taken on the ordinate axis is double the route taken on the abscissa axis, which leads to a moving system that does not stop, so the torque $T = 1.20$ $Newton.meter$ does have enough force to move the system in permanent regime.

According to Fig. 11, the resulting reaction is different from $zero$, denoted by $R_R \neq 0$, which results in the crank-connecting rod system not stopping; that is, a cyclic movement is presented,

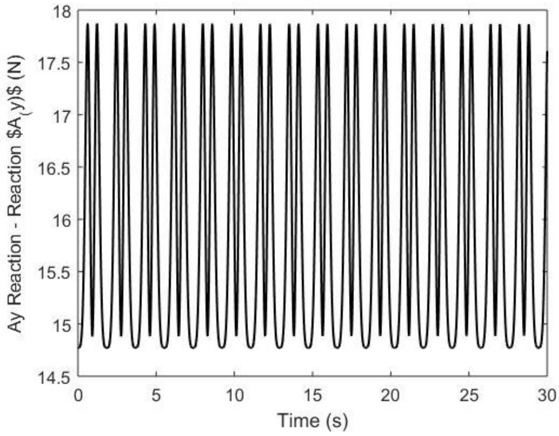

Figure 10: Resulting reaction on the y-axis on the system

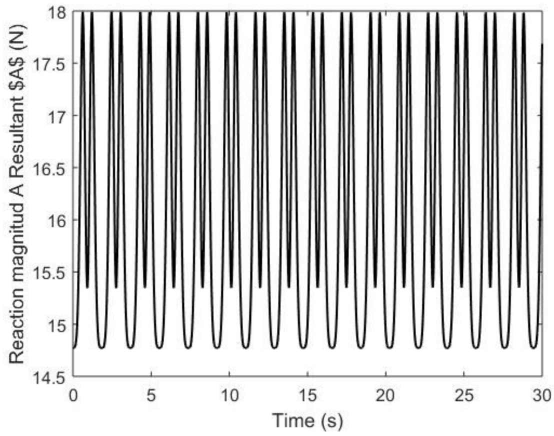

Figure 11: Magnitude Resulting reaction R_R on the system

which implies that the torque $T = 1.20$ $Newton.meter$ does have enough force to move the system in a permanent regime, without reaching an underdamped behavior. The resultant reaction is structured by the square root of $R_x^2 + R_y^2$ being R_x is the resultant component along x axis and R_y is the resultant component along y axis.

According to Fig. 12 the input torque is the result of the action of a crank a of length 0.2 $meters$, mass $m_1 = 1.6$ kg, connecting rod L of length 0.6 meters, considering a coefficient of fluctuation of the angular velocity with respect to the average value $k = 0.02985$, viscous friction constant $c = 0.00001$, acceleration of gravity $g = 9.81$ m/s^2, and maximum angular velocity $\dot{\alpha} = 3.4$ rad/s as shown in Fig. 7. The dashed curved line represents the input torque to the mechanism without flywheel with a maximum value of 1.6 $Newton.meter$; that is, the required torque is equivalent to 1.6 $Joules$ of energy to move the system under the given conditions. The continuous curved line represents the input torque to the mechanism with flywheel with a value of 0.1 $Newton.meter$; which means the torque required is 0.1 $Joules$ of energy to move the system under the stated conditions.

According to Fig. 13, a relationship between the three parameters is obtained: mass m of the flywheel in $kilograms$, thickness and internal mass of the flywheel in $meters$, and external radius r_o of the flywheel in $meters$. It can be observed that by varying the value of thickness e, both the external radius of the flywheel and mass m of the same will vary.

The selection m, r_o and e of the flywheel will serve to determine the optimal construction of the flywheel according to the established parameters, considerations, and relationships, as shown in Table 1.

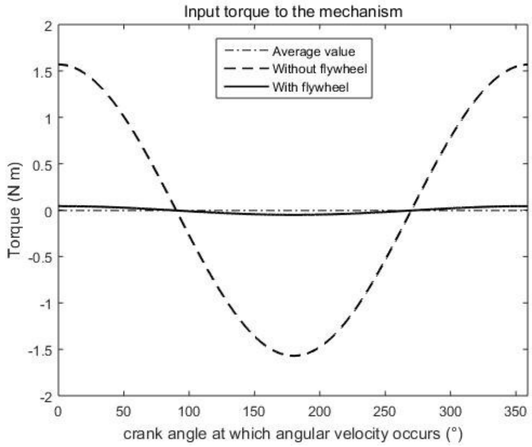

Figure 12: Input torque to the system with and without flywheel

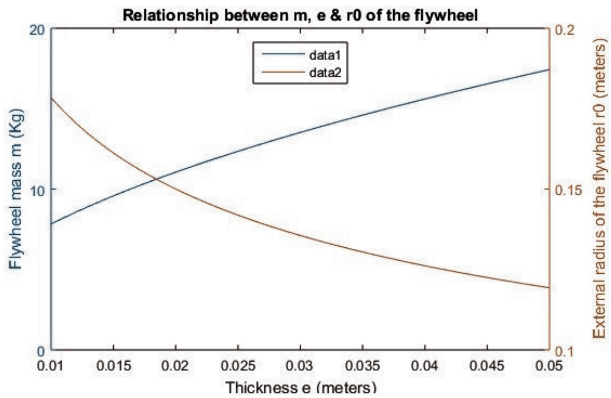

Figure 13: Relationship between mass m, thickness e and external radius r_0 of the flywheel

From (39) and table 2: $\triangle E_C = E_{\dot{\alpha}}max - E_{\dot{\alpha}}min = +1.6$ J - 0.1 J = + 1.5 J
From (40): $k = \frac{\dot{\alpha}_{max}-\dot{\alpha}_{min}}{\dot{\alpha}_{prom}} = \frac{3.4-3.3}{3.35} = 0.02985$
From (41): $I_{system} = \frac{|\triangle E_c|}{k.\dot{\alpha}^2_{prom}} = \frac{|+1.5N.m|}{0.02985.(3.35\frac{rad}{s^2})^2} = 6.716585\ kg.m^2$
From (42): $I_{crank} = \frac{1}{3}.m_1.a^2 = \frac{1}{3}.(1.6kg).(0.2m)^2 = 0.021333\ kg.m^2$
Replacing in (43) we obtain:

The difference between the first two moments corresponded to the moment of inertia of the flywheel, as listed in Table 3.

It can be seen that with the analysis of the mass, density in a crank-connecting rod mechanism with respect to (Beltrán, 2022; Carrillo, 2022) and parameters such as mass, density, outer radius, thickness of a flywheel in the case of composite materials (Premkumar et al., 2021), in the case of electric motors (Lamichhane et al., 2025) and green technologies (Zhang & Fujii, 2025) the system can be optimized in what corresponds to the moment of inertia without neglecting the coefficient of fluctuation of the angular velocity k, the viscous friction constant c, the acceleration of gravity g, with the consideration of the corresponding kinematic conditions by using a highly nonlinear second-order differential equation for the angular acceleration provided by a crank-connecting rod system, through an inverse dynamic analysis as well as the moment

Table 1: Proportionality relationship between m, e, r_o of the flywheel

mass	proportionality	thickness	proportionality	External radius
m	direct	e	inverse	r_0

Table 2: Energy analysis in the behavior of Torque vs. crank angle α

Segment	Amplitude	Interval	Kinetic energy	Energy	Accumulated
AB	1.6 - 0	0 - $\frac{\pi}{2}$	(1.6N.m),0,$\frac{3\pi}{2}$	+1.6 Joules	+1.6 Joules
BC	0-(-1.65)	$\frac{\pi}{2}$-$\frac{3\pi}{2}$	(1.65N.m),$\frac{\pi}{2}$,$\frac{3\pi}{2}$	-3.3 Joules	-1.7 Joules
CD	0 - 1.6	$\frac{3\pi}{2}$-2π	(1.6N.m),$\frac{3\pi}{2}$,2π	+1.6 Joules	-0.1 Joules

Table 3: Moment of inertia resulting from the flywheel in $kg.m^2$

I_{system}	I_{crank}	$I_{flywheel}$
6.716585	0.021333	6.695251

of inertia of the mechanism, the equations of motion of the connecting rod and the crank, and the flywheel equation.

In summary, the results obtained were:

• It is shown that the system without a flywheel exhibits fluctuations in angular velocity and input torque.

• With the flywheel, the angular velocity is more stable and the required torque is reduced.

• The kinetic energy varies by 1.5 Joules without the flywheel, while with it, it remains more constant.

• The relationship between the system's moment of inertia and the flywheel allows for the design of a more efficient system.

There are no conflicts of interest, but on the contrary, they contribute to the development and progress of the use of materials for the construction of flywheels. All funding was provided by the researcher.

4 Conclusions

According to Fig. 10, for a mass $m_1 = 1.6\ kg$ with a crank of length $a = 0.2\ meters$, a torque of 1.2 $Newton.meter$, with a connecting rod of length $L = 0.6\ meters$, acceleration of gravity $g = 9.81\ m/s^2$, with a coefficient of friction or constant proportion $c = 0.00001$ dimensionless A maximum angular velocity of 3.4 rad/sec is obtained, a maximum angular acceleration of 24 rad/s^2, a maximum resultant reaction Rx of 3.7 $Newtons$, a maximum resultant reaction Ry of 17.8 $Newtons$, a resultant reaction R_R of 18 $Newtons$, which establishes the constant movement of the mobile (Jia et al., 2025) using a crank-connecting rod system for an external torque in point A of $T = 1.2\ Newtons$. The mass m_2 of the BC part or the connecting rod L can be ignored. Obtaining a significantly smoother torque using a flywheel (Akhtar, 2024) avoids the extreme values (Kumar, 2023).

In summary, the conclusions were:

• The use of a properly sized flywheel improves the system's energy efficiency.

• Motor oversizing is avoided, reducing energy waste.

• Future studies are proposed to optimize material selection and flywheel design for applications in vehicles and other rotational systems considering equilibrium between mass thickness and external radius of the flywheel.

5 Acknowledgement

I would like to thank Dr. Raúl Ricardo Sulla Torres for his unconditional support throughout this complex research journey, Dr. Manuel Alfredo Alcázar Holguin for his wise and timely advice on my path to academic growth, and the Universidad Nacional de San Agustín de Arequipa, Arequipa, Peru.

References

Akan, A., Chaparro (2024). *Signals and Systems Using MATLAB. Elsevier.*

Akhtar, J. (2024). Enhancing Electric Vehicle Performance & Battery Life through Flywheel Energy Storage System Modelling Simulation & Analysis. *Symposium on International Automotive Technology*, (p. 8). Pune, India: SAE International.

Bayram, B., Samuel, S. (2025). Evaluation of Thermal Performance of the Motor Generator Unit-Kinetic (MGU-K) for 2026 Formula 1 Power Unit Regulations. *SAE Technical Paper.*

Beckers, J., Verstraten, T., Verrelst, B., Contino, F., & Van Mierlo, J. (2021). *Analysis of the Dynamics of a Slider-Crank Mechanism Locally Actuated with an Act-And-Wait Controller. Mechanism and Machine Theory.* Brussels, Belgium: Vrije Universiteit Brussel.

Beltrán, S. (2022). *Optimización Topológica Multifase Sobre Diseño Generativo de Biela de Motor de Combustión Interna a Través del Software Inventor* [Tesis de Titulación, Universidad Internacional del Ecuador]. Guayaquil. Ecuador: `https://repositorio.uide.edu.ec/bitstream/37000/5016/1/T-UIDE-0348.pdf2022.`

Campanelli, M., dÁlfonso, A., Tacconis, C., Caprioglio, E., Scarpa, L., Tayyab, M., & Pérez, S. (2020). *Classical Mechanics.* Bristol, United Kingdom: Institute of Physics Publishing Ltd.

Carrillo, F. (2022). Optimización topológica de una biela de motor de combustión interna utilizando elemento finito. *Creación Artística, Tecnológica, Humanidades e Investigación Científica*, `https://cathi.uacj.mx/handle/20.500.11961/22061?show=full.`

Coelho, R.L. (2018). On the deduction of Newton's second law. *Acta Mechanica*, *229*(5), 2287-2290.

Chmielowiec, A., Woś, W., & Czyżewski, J. (2025). Numerical Analysis of Inertia Forces in the Connecting Rod and Their Impact on Stress Formation. *Materials, 18*(6), 1385. `https://doi.org/10.3390/ma18061385`.

Drápal, L., Novotný, P. (2017). Torsional vibration analysis of crank train with low friction losses. *Journal of Vibroengineering*, *19*(8), 5691-5701.

Hu, Y., Wei, Y., & Liu, M. (2021). Design and performance evaluation of a spherical robot assisted by high-speed rotating flywheels for self-stabilization and obstacle surmounting. *Journal of Mechanisms and Robotics, 13*(6), 061001.

Jia, D., Liu, Y., Lei, J., Deng, X., Deng, W., & Ji, H. (2025). Design and Kinematic Characterization of Connecting Rod Set for Variable Compression Ratio Engines. *Energies*, *18*(5), 1276.

Kaveh, A., Ilchi Ghazaan, M. (2017). A new meta-heuristic algorithm: vibrating particles system. *Scientia Iranica, 24*(2), 551-566.

Khudhair, M.R., Kamil, F., Kadhom, M.A., & Gburi, F.H. (2024). Optimum Design of Connecting Rod–A Review. *Journal of Mechanical Design, 11*(1), 1-9.

Kumar, D.P., Paswan, A.K. (2023). Design and Statical Structural Analysis of Connecting Rod Using Different Material. *IJRAR-International Journal of Research and Analytical Reviews (IJRAR), 10*(4), 770-781.

Lamichhane, T., Wang, H., Chinnasamy, C., Sethuraman, L., List, F., Nandwana, P., & Paranthaman, M. (2025). An Additively Manufactured Fe-3Si Stator for a High-Performance Electrical Motor. *Applied Sciences*, *15*(4), 1706.

Liang, X.M., Xing, Y.Z., Li, L.., Yuan, W.K., & Wang, G.F. (2021). An experimental study on the relation between friction force and real contact area. *Scientific Reports, 11*(1), 20366.

Lindner, A., Strauch, D. (2018). *A complete course on theoretical physics. From Classical Mechanics to Advanced Quantum Statistics*. Cham, Switzerland: Springer.

Lu, Z., Ren, Y., Liu, Ch., Chen, S. & Zhao, Y. (2025). Design, Analysis, and Flexibility Evaluation of a Double-Mode Underactuated Coupled-Drive Omnidirectional Mobile Robot, *Journal of Robotics,* https://doi.org/10.1002/rob.22574.

Nkomo, N.Z., Alugongo, A.A. (2024). Flywheel Energy Storage Systems and Their Applications: A Review, *International Journal of Engineering Trends and Technology*, *72*(4), 209-215.

Premkumar, T., Vali, D., Sai, A., Sudarshan, P., Roopak, P., Hariram, V., & Seralathan, S. (2021). Optimizing the Design and Material used for Connecting Rod through Finite Element Simulation. *International Journal of Vehicle Structures and Systems*. https://doi.org/10.4273/ijvss.13.5.02.

Rasha, A., Machicao, S. (2023). *Flywheels. Energies.*

Reyes, G., Cañizares, F., Villacres, A., & Noroña, M. (2017). Análisis mecánico del brazo de biela mediante norma ASTM e8, *INNOVA*, *2*(5), 190 - 204.

Steau, E., Mahendran, M., & Poologanathan, K. (2020). Elevated temperature thermal properties of carbon steels used in cold-formed light gauge steel frame systems, *Journal of Building Engineering*, 28, 101074.

Urbaś, A. Stadnicki, J. (2025). Applications of dynamics metamodels of an eccentric crank-slider mechanism in the initial phase of their design. *Mechanism and Machine Theory*, 205. https://doi.org/10.1016/j.mechmachtheory.2024.105886.

Zhang, B., Yan, Y., Dong, X., Dykman, M.I., & Chan, H.B. (2024). Frequency stabilization of self-sustained oscillations in a sideband-driven electromechanical resonator. *American Physical Society*, https://journals.aps.org/prapplied/pdf/10.1103/PhysRevApplied.22.034072.

Zhang, X., Lian, B., Shen, H., Cheng, S., & Li, F. (2025). Challenges and Strategies for Multi-Electron Reactions in High-Energy Phosphate-Based Cathodes for Sodium-Ion Batteries. *Advanced Functional Materials*, 2420864.

Zhang, Z., Fujii, H. (2025). A Global Analysis of Patent Invention Strategies in Automotive Technologies for Environmental Sustainability. *Sustainability*, *17*(2), 696.

Zhao, B., Wang, S., Xiao, P., Xu, L., Hu, X., Si, X. & Liu, Y. (2022). The Tribo-Dynamics Performance of the Lubricated Piston Skirt–Cylinder System Considering the Cylinder Liner Vibration, *Lubricants. 10*(319). https://doi.org/10.3390/lubricants10110319.